Delay dynamics of semiconductor lasers with short external cavities: Bifurcation scenarios and mechanisms

T. Heil, I. Fischer, and W. Elsäßer
Institut für Angewandte Physik, Technische Universität Darmstadt, Schloßgartenstraße 7, D-64289 Darmstadt, Germany

B. Krauskopf and K. Green
Department of Engineering Mathematics, University of Bristol, Bristol, United Kingdom

A. Gavrielides
Nonlinear Optics Center, Air Force Research Laboratory AFRL/DELO, 3550 Aberdeen Avenue SE, Kirtland AFB, New Mexico 87117-5776, USA

(Received 15 January 2003; published 26 June 2003)

We present a comprehensive study of the emission dynamics of semiconductor lasers induced by delayed optical feedback from a short external cavity. Our analysis includes experiments, numerical modeling, and bifurcation analysis by means of computing unstable manifolds. This provides a unique overview and a detailed insight into the dynamics of this technologically important system and into the mechanisms leading to delayed feedback instabilities. By varying the external cavity phase, we find a cyclic scenario leading from stable intensity emission via periodic behavior to regular and irregular pulse packages, and finally back to stable emission. We reveal the underlying interplay of localized dynamics and global bifurcations.

DOI: 10.1103/PhysRevE.67.066214 PACS number(s): 05.45.Jn, 42.65.Sf, 42.55.Px

I. INTRODUCTION

Understanding the influence of delayed optical feedback on the behavior of semiconductor lasers is of great relevance for technological applications, where the feedback is typically due to unwanted external reflections. Such feedback tends to destabilize semiconductor lasers, an effect known as coherence collapse [1], so that expensive optical isolators often have to be introduced. On the positive side, it has been demonstrated that chaotic output of a semiconductor laser with optical feedback can be constructively used for functional purposes, for example, as carriers for encrypted optical communication schemes [2–6]. From a theoretical point of view, lasers with delayed optical feedback are very interesting because they can be modeled successfully by delay differential equations (DDEs) [7–9]. This class of dynamical systems has recently been the subject of intense activity because DDEs also appear as models in applications ranging from control schemes [10] and neural networks [11] to biological systems [12]. It is an inherent feature of DDEs that they have an infinite-dimensional phase space, which makes them much harder to treat analytically than ordinary differential equations. Arguably, the experimental efforts towards characterization and understanding the dynamics of semiconductor lasers with delayed optical feedback have been driving forces behind recent theoretical research of complex dynamics and bifurcations of DDEs [13–19].

We consider a fundamental and long-standing problem: understanding the dynamical behavior of a semiconductor laser experiencing delayed optical feedback from an external mirror. This problem has been studied extensively, both experimentally and theoretically for more than two decades; for some recent surveys see Refs. [21,20], and references therein. In most studies long external cavities with lengths from about 10 cm to several meters have been considered. The dynamics of the long external cavity configuration includes the often studied phenomena of low-frequency fluctuations (LFFs) and coherence collapse; see, for example, Ref. [22].

In this paper, we focus on the *short cavity regime* as recently introduced in Ref. [23]. Our study is motivated from several different points of view. First of all, short external cavities are dominant in technological applications, in particular, in data storage and telecommunication modules. Furthermore, the study of the dynamics in this regime has become experimentally accessible with the recent development of faster real-time measuring technology. From the dynamical systems point of view, the short external cavity regime is very interesting because it is of an intermediate complexity. This is an advantage in direct modeling and also allows for the application of theoretical bifurcation tools for DDEs that have become available only very recently [13,17].

We give a comprehensive analysis of the short external cavity regime by combining experimental characterization, modeling, and bifurcation analysis. This allows us to present a consistent overall picture of the dynamics and, at the same time, present detailed bifurcation scenarios, involving local and global bifurcations, of how complicated dynamics develop from stable laser output. We present the experimental demonstration of a dynamical scenario evolving under variation of the optical feedback phase accumulated within the external cavity. Within one 2π-periodic cycle of the cavity phase, we find a scenario leading from stable intensity emission via periodic emission to a complicated state made up of irregular and regular pulse packages back to stable emission. This scenario represents a major characterizing feature of the short cavity regime.

The dynamical scenario, as well as the individual dynamical states can be modeled in excellent agreement to the experiments by the Lang-Kobayashi equations [24], providing insight into the occurrence of localized and global orbits.

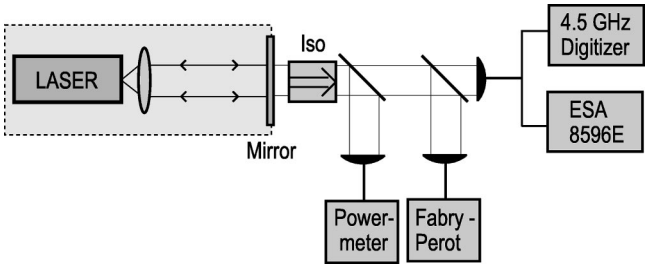

FIG. 1. Schematic of the experimental setup.

Finally, alternative methods for studying the bifurcation mechanisms have been applied to the same model equations, unveiling the phase space structure and relevant bifurcation mechanisms. Bringing all this together, we are able to explain the scenario as a delicate interplay between localized dynamics and a global reinjection mechanism, which becomes available to the system as a result of global bifurcations.

The paper is organized as follows. A detailed experimental characterization of the dynamical scenario is presented in Sec. II. In Sec. III, we introduce the Lang-Kobayashi (LK) equations and study their solutions by numerical simulations. Detailed insight into the underlying bifurcations is presented in Sec. IV by means of computing unstable manifolds of external cavity antimodes. We draw conclusions and point to open questions in Sec. V. The Appendix contains more background material on the LK equations.

II. EXPERIMENT

Our experiments aim to provide a detailed characterization of the dynamics of a semiconductor laser operating in the short cavity regime. Particular emphasis is put on the question of how these dynamics depend on variation of the optical feedback phase. We use the experimental setup depicted in Fig. 1 in order to resolve the different time scales and wide range of optical frequencies present in the dynamics of the system.

The semiconductor laser is a Sharp LT015MDO laser, operating at a solitary wavelength of $\lambda = 837$ nm. The SL is pumped by an ultra-low-noise current source and its temperature is stabilized to better than 0.01 K. The solitary laser threshold amounts to $J_{th,sol} = 41.7$ mA. The external cavity is formed by an aspheric lens collimating the laser beam, and a semitransparent dielectric mirror with a reflectivity of 90%. Towards the external cavity, the laser is antireflection coated with $\approx 10\%$ reflectivity, the other facet is high-reflection coated with $\approx 90\%$ reflectivity. At optimum alignment of the external cavity, we achieve a maximum threshold reduction of 11.5%. The length of the external cavity has been varied between 5 cm and 1.1 cm, which corresponds to external cavity round-trip frequencies of the light between $\nu_{EC} = 3$ GHz and $\nu_{EC} = 14$ GHz, respectively.

Our detection scheme provides an excellent temporal resolution of the intensity dynamics of the system. We detect the light transmitted through the semitransparent mirror using a fast photoreceiver of 8 GHz bandwidth. The signal of the photoreceiver is amplified by broadband amplifiers, and transferred to a Tektronix SCD5000 fast digitizer with an analog bandwidth of 4.5 GHz and a HP 8596E electrical spectrum analyzer with a 6 GHz bandwidth. This large detection bandwidth allows us to record single shot measurements resolving the fast round-trip oscillations of the light for substantial ranges of the investigated external cavity lengths. Simultaneously, to the intensity dynamics, we record the optical spectrum of the laser using a Newport SR-240-C Fabry-Perot-type optical spectrum analyzer. In addition, we detect the time averaged laser intensity using a slow photodiode and monitor its signal with a power meter. Finally, the optical isolator (Iso) shields the external cavity configuration from perturbations from the detection branch.

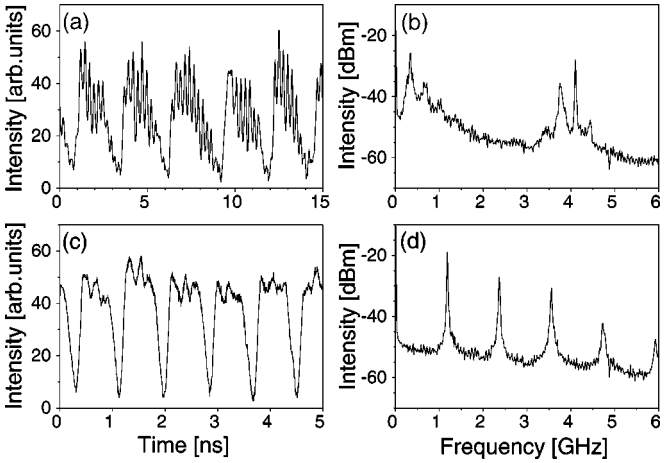

FIG. 2. Pulse packages in the intensity dynamics of a semiconductor laser operating in the short cavity regime. The time series in panel (a) and the corresponding rf spectrum in panel (b) were recorded for an external cavity length of 3.7 cm and an injection current of $1.08 I_{th,sol}$; the external cavity round-trip oscillations of $\nu_{EC} = 4.1$ GHz are fully resolved in the time series. The time series in panel (c) and the rf-spectrum panel (d) were recorded for an external cavity length of 1.1 cm and an injection current of $1.8 I_{th,sol}$; the external cavity round-trip oscillations of approximately $\nu_{EC} = 14$ GHz are not fully resolved in the time series.

A. Pulse packages

The external cavity lengths selected in our experiments lead to feedback induced instabilities that have been summarized recently as the *short cavity regime* (SCR) [23]. The SCR is entered as soon as the external cavities are sufficiently short, such that the external cavity frequency ν_{EC} substantially exceeds the solitary laser relaxation oscillation frequency ν_{RO}. A striking dynamical phenomenon present in the SCR is the formation of *pulse packages* (PP) in the laser intensity. Figure 2 presents two characteristic examples of PP intensity time series, and their corresponding rf spectra for two different external cavity lengths, and injection currents.

Figure 2(a) shows that a single PP consists of a series of pulses occurring regularly at ν_{EC}. The pulse intensities are modulated by a low-frequency envelope that forms the individual pulse packages. Beginning with a sudden light burst constituting the first dominant pulse of the package, the energy of the individual pulses gradually decreases with time

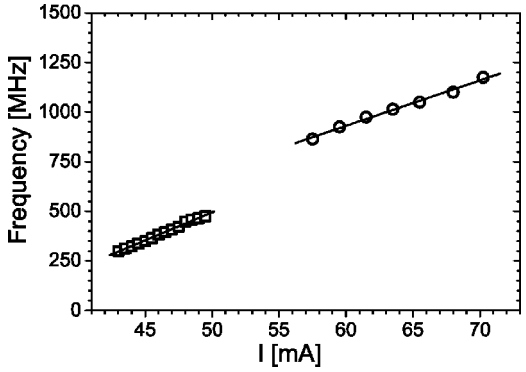

FIG. 3. Dependence of the RPP envelope frequency ν_{RPP} on the injection current. The squares represent the results for an external cavity with $\nu_{EC}=4.1$ GHz, the circles represent the data for the cavity with $\nu_{EC}=14$ GHz. The lines are linear fits to the experimental data.

until the laser intensity drops almost to zero, marking the time interval before the next dominant light burst. The corresponding rf spectrum, depicted in Fig. 2(b), exhibits a low- and a high-frequency part. The low-frequency part consists of a dominant peak corresponding to the repetition frequency of the PP at $\nu_{PP}\approx 330$ MHz and its harmonics. The high-frequency part of the rf spectrum consists of a dominant peak at ν_{EC} with side peaks separated by ν_{PP}. Accordingly, panel (b) underlines that the PP represent a low-frequency phenomenon in the dynamics of the system, since $\nu_{PP} \ll \nu_{EC}, \nu_{RO}$. Figure 2(c) demonstrates that the PP phenomenon is robust against substantial variations of the external cavity length and the injection current. Although the individual external cavity round-trip pulsations are not resolved here, the characteristic envelope of the PP is still clearly visible. Also due to detection bandwidth limitations, Fig. 2(d) only shows the low-frequency part of the corresponding rf spectrum, that is, the very sharp PP peak and its harmonics. This shows that the PP can develop a well-defined repetition frequency. The dynamical regime in Figs. 2(c) and 2(d) has also been referred to as *regular pulse packages* (RPP) [23]. Thus, the RPP are characterized by two distinct frequencies. While it is clear that the repetition frequency of the fast pulsations is determined by the external cavity round-trip frequency ν_{EC}, it is an open question where the RPP envelope frequency ν_{RPP} originates from. We address this open question by analyzing the injection current dependence of ν_{RPP}. Figure 3 depicts the observed current dependence of the RPP frequency obtained from the rf spectra. Data for two different external cavity lengths is shown, which correspond to those of Fig. 2. Squares represent the results for an external cavity with $\nu_{EC}=4.1$ GHz, circles represent the results for the cavity with $\nu_{EC}=14$ GHz.

We find a linear dependence of ν_{RPP} on the injection current. Furthermore, we give evidence that this linear dependence is independent of the cavity length, thus being a characterizing feature of the RPP dynamics. The linear scaling is remarkable because the solitary relaxation oscillation frequency shows a square-root scaling with $\nu_{RO}\sim\sqrt{I-I_{th}}$. Thus, the RPP envelope frequency ν_{RPP} cannot be simply associated with the relaxation oscillation frequency ν_{RO}. In addition, ν_{RPP} is significantly smaller than ν_{RO}. In conclusion, the linear scaling and the slow time scales of the RPP envelope frequency ν_{RPP} already indicate that not the solitary laser characteristics, but rather the structure of the phase space and the corresponding unstable manifolds govern the dynamics of the PP.

B. Role of the feedback phase

The hallmark distinguishing the dynamics in the SCR from the dynamics in the long cavity regime (LCR) is the sensitivity on the optical feedback phase. In the LCR, we never observed an influence of the feedback phase for any laser with optical feedback. Only the synchronization behavior of two separated lasers with optical feedback allows one to detect its influence [30]. However, in the SCR, as we demonstrate in this paper, the emission dynamics indeed depend very sensitively on the feedback phase, which is, thus, identified as a key parameter.

Our experiments represent the systematic study of the influence of the optical feedback phase on the dynamics of semiconductor lasers operating in the SCR. The optical feedback phase exhibits a particular cyclic nature. Starting from a certain initial state, a variation of the optical feedback phase by 2π must lead back to this initial state. This point will be discussed in detail in Sec. II C. We demonstrate that the dynamical scenario evolving under variation of the optical feedback phase exhibits a 2π-cyclic behavior. The scenario leads to a series of bifurcations from stable emission to PP and back to stable emission after a phase variation of 2π. In this section, we focus on the experimental results and merely hint at the possible underlying dynamics. A detailed numerical and bifurcation analysis of this cyclic scenario is the topic of Secs. III and IV.

Experimentally, a well controlled variation of the optical feedback phase can be implemented in the following two ways. First, the feedback phase can be controlled by changing the external cavity length on the optical wavelength scale using a piezo transducer. Accordingly, the feedback phase can be varied over the whole 2π interval, while the resulting changes of the external cavity length are small and can be neglected. Second, the feedback phase can be shifted by tuning the emission wavelength, while keeping the external cavity length constant. Already small changes of the injection current are sufficient to tune the emission wavelength of the laser such that the optical feedback phase is shifted by 2π. Again, the influence of this phase shifting method on other parameters is negligible. In the experiments, we choose the injection current tuning because our setup allows a very accurate control of this parameter.

Varying the feedback phase via the injection current, we find that on regular intervals of ≈ 2.5 mA width, the PP state disappears in favor of a stable emission state in which the laser operates on a single external cavity mode (ECM). Within these intervals, we observe a characteristic dynamical scenario leading from stable emission back to the PP state. For an external cavity length of 1.1 cm, we observe eight full cycles of this scenario until, finally, the PP state is no longer

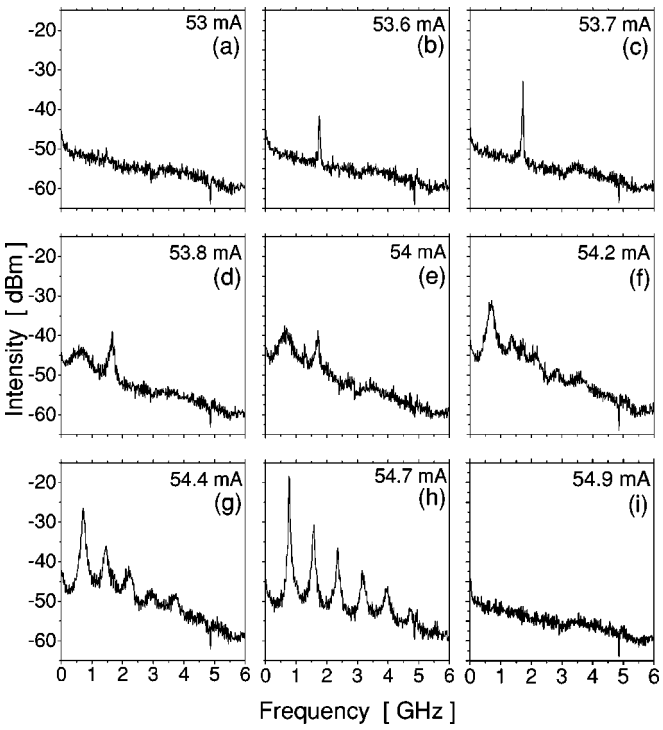

FIG. 4. One cycle of the repeating dynamical scenario characterized by the rf spectra of the laser emission. The external cavity length is 1.1 cm and the threshold reduction 11.5%. The injection current is indicated on each panel.

lost and a continuous transition from RPP to an irregular pulsating behavior takes place. Finally, we note that the excellent agreement between our experimental measurements and our numerical and analytical results confirms the validity of the chosen experimental method. The following section provides a detailed characterization of a full cycle of the dynamical scenario.

C. Scenario of one feedback phase cycle

The dynamical scenario mediating between stable emission and the RPP is best characterized by analyzing the rf spectra of the laser emission. Figure 4 presents a sequence of rf spectra over one full cycle of the dynamical scenario.

Figure 4(a) depicts a flat rf spectrum corresponding to stable emission on a single ECM. The corresponding Fabry-Perot spectrum displays a single line, confirming single-mode emission. Suddenly, after increasing the injection current by a few tenths of milliamperes, a single sharp peak at 1.7 GHz appears in the rf spectrum, shown in Fig. 4(b). This peak corresponds neither to the RPP frequency nor to the solitary relaxation oscillation frequency. Upon further increasing the injection current, this peak gains in amplitude and is shifted to slightly lower frequencies; see Fig. 4(c). The peak in the corresponding optical spectrum now exhibits sidebands at a distance given by its frequency in the rf spectrum. This transition is consistent with the signature of a Hopf bifurcation. When the injection current is increased further, a second, strongly broadened peak appears in the low-frequency part of the rf spectrum at ≈ 700 MHz; see Fig. 4(d). Also, the remainder of the first peak is now broadened. This behavior suggests the creation of a much larger attractor. The Fabry-Perot interferometer no longer displays distinguishable peaks. This indicates that the laser emits on several longitudinal diode modes and a large number of ECMs.

Figures 4(e) and 4(f) show that, as the injection current is increased, the amplitude of this new peak grows and its frequency decreases. Simultaneously, the amplitude of the peak at 1.6 GHz diminishes, until it finally vanishes. The low-frequency peak now dominates the rf spectrum of Fig. 4(f). In Fig. 4(g), the low-frequency peak has further increased in amplitude and narrowed in frequency width; its harmonics are clearly visible. The time series now displays the typical PP behavior of Fig. 2. As the feedback phase is further shifted towards 2π, the regularity of the PP increases and regular pulse packages (RPPs) appear: the rf spectrum in Fig. 4(h) shows that the dynamical range of the main peak increases to more than 30 dB and its full width at half maximum has reduced to 3 MHz. Finally, as pictured in Fig. 4(i), the dynamical scenario concludes in a sudden disappearance of the RPP state, which is then replaced by stable emission on a single ECM. This transition depicted in Figs. 4(h) and 4(i) is not only sudden but also displays *hysteresis*: the transition from the RPP to stable emission occurs at higher injection currents than the transition from stable emission back to the RPP state.

In the following sections, we will confirm by numerical and theoretical investigations the dynamics underlying the transitions over one cycle of the feedback phase depicted in Fig. 4.

III. MODELING

The Lang-Kobayashi (LK) equations [24] are model equations that have been used extensively in the past to describe a semiconductor laser subject to feedback from an external cavity; see also Ref. [20]. For long external cavities, they are able to describe the statistics of the fast pulsations [25] as well as the statistics and the pump dependence of the low-frequency fluctuations [26]. For short external cavities, it has recently been shown that the LK equations can also explain the onset of regular pulse packages [23].

Nevertheless, the LK equations include some approximations that have to be carefully deliberated when comparing modeling with the experimental data. The LK equations are a model that accounts only for one longitudinal mode of the solitary laser. It has been found that, when analyzing the modal behavior of multimode lasers, phenomena beyond the LK description such as antiphase dynamics can occur [27,28]. The LK model neglects multiple reflections, therefore one has to be careful when considering strong feedback. Furthermore, the LK model does not consider the spatial extension of the laser. Strongly asymmetric facet reflections can lead to effects such as jump-ups that are not being captured by the LK model [29].

We are aware of these limitations but, nevertheless, choose the LK model for our modeling and analysis for two reasons. First, we aim for a comprehensive study of the bifurcations and mechanisms, and this requires a not too complicated model. Second and more importantly, the LK model

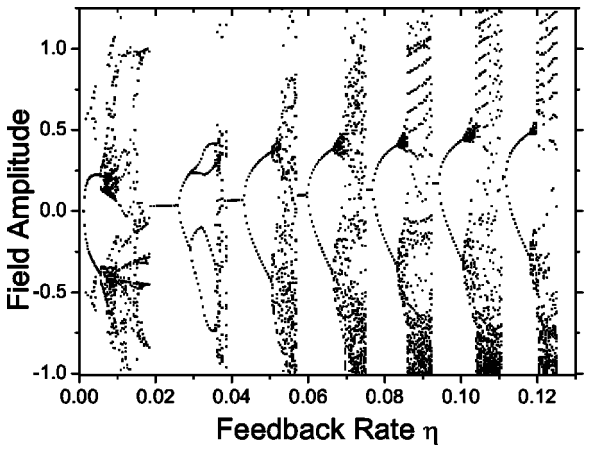

FIG. 5. Bifurcation diagram of the field amplitude; plotted are $\max(R/\sqrt{P}-1.0)$ and $\min(R/\sqrt{P}-1.0)$ as a function of feedback strength η for the parameter values $T=1710$, $\alpha=5.0$, $P=0.8$, $\tau=70$, and $C_p=0.0$.

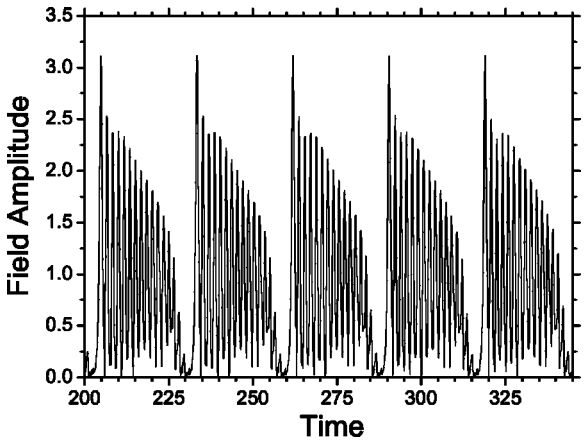

FIG. 6. Time series of the amplitude of the RPP. The time has been normalized to the relaxation frequency of the laser, $\omega_r=\sqrt{2P/T}$. The parameter values are $T=1710$, $\alpha=5.0$, $P=0.8$, $\tau=70$, $C_p=\pi$, and $\eta=0.115$.

gives excellent agreement with the experimental findings that were discussed in Ref. [23] and with those in this paper. In other words, the results presented here strongly suggest that the LK equations describe even complex phenomena in the short cavity regime remarkably well.

As was done previously in Ref. [23], we write the LK equations as the dimensionless and compact set of equations

$$\frac{dE}{dt}=(1+i\alpha)NE+\eta E(t-\tau)e^{-iC_p}, \tag{1}$$

$$T\frac{dN}{dt}=P-N-(1+2N)|E|^2, \tag{2}$$

for the (normalized) electric field E and inversion N. See the Appendix, Eqs. (A1) and (A2), for a version of these equations in terms of physical parameters and including a normalization procedure to derive Eqs. (1) and (2).

Here, we briefly discuss the Lang-Kobayashi equations within the context of the experiment and emphasize some of the interesting solutions that can be found in the short cavity regime. Equations (1) and (2) describe a semiconductor laser with external optical feedback. We assume single longitudinal mode operation, even though in the experiment the laser when unstable oscillates on a number of modes. In addition, multiple external cavity round trips have been ignored as the facet of the laser facing the external mirror is AR coated. Also, we have neglected gain saturation and cross-saturation effects. Our interest is to obtain a physical understanding of the bifurcation phenomena rather than to model the system exactly by including all possible details.

We first investigate the development of the dynamics to full RPP as a function of the feedback strength η. In Fig. 5, we show the maxima, $\max(R/\sqrt{P}-1.0)$, and minima, $\min(R/\sqrt{P}-1.0)$, of the normalized deviation from the solitary laser steady state of the amplitude of the electric field as a function of the feedback strength η. To ensure that the respective attractor was reached in Fig. 5 (and also in Fig. 7 below), a transient of 5000 normalized time units was discarded for every value of η and then the maxima and minima were plotted over the next 200 normalized time units. (The calculations swept forward and backward to catch any hysteresis, especially for Fig. 7.) The remaining parameters are held fixed at $T=1710$, $P=0.8$, $\tau=70$, $\alpha=5.0$, and $C_p=0.0$. These parameters are chosen not only to elucidate the bifurcation structure, but also correspond fairly well to the experimental conditions. Very similar values of the parameters were also used in Ref. [23]. The sequence of ECMs, each depicted as a single point for a given value of η, can be clearly seen. Each mode, starting with the mode that emerges from the solitary laser mode, undergoes a sequence of bifurcations to chaos.

Typically the first few modes exhibit a Hopf bifurcation followed by a period-doubling bifurcation. However, modes appearing at larger feedback rates show a Hopf bifurcation followed by a torus bifurcation, leading to quasiperiodic solutions. Further, the torus in these modes suddenly disappears and a state that seems to be fairy regular, but with a large pulsating amplitude appears. This is a PP state that

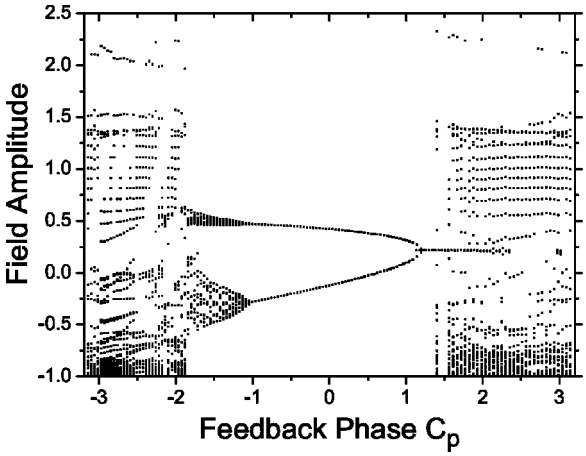

FIG. 7. Bifurcation diagram of the field amplitude, where we plotted $\max(R/\sqrt{P}-1.0)$ and $\min(R/\sqrt{P}-1.0)$ as a function of $C_p\in[-\pi,\pi]$ at $\eta=0.115$. The other parameters are as in Fig. 6.

persists in an interval of feedback strength, before the next high-gain mode becomes available through a saddle-node bifurcation and to which the laser eventually settles. This particular bifurcation diagram is very sensitive to the phase of the delay. When this crucial parameter is changed, one finds a very similar structure of bifurcation cascades, but the particular values of the feedback rate at which the various bifurcations take place is altered significantly.

Numerically obtained RPP for the parameter values as above, but with $C_p=\pi$ at $\eta=0.115$ are shown in Fig. 6. There are two fundamental frequencies, the one corresponding to the pulsations is at the external cavity frequency, the other and much lower corresponds to the envelope of the RPP. The RPP is very regular and the trajectory variations from pulse package to pulse packages are very small.

To illustrate the effect of the feedback phase and its sensitive influence on the different types of attractors, Fig. 7 shows the maxima and the minima of the normalized amplitude as a function of $C_p \in [-\pi,\pi]$ for $\eta=0.115$. The values of the other parameters have been kept fixed at their previous values. For some positive values of C_p, the laser is operating in the maximum-gain mode (MGM). As the phase is decreased the laser undergoes a Hopf bifurcation to a limit cycle leading to a distinct single frequency in the rf spectra as in Figs. 4(b) and 4(c). The laser then undergoes a torus (or secondary Hopf) bifurcation to a torus over a rather small interval of the feedback phase. Suddenly at $C_p=-1.95$, the attractor increases dramatically and the laser is found to produce pulse packages. These pulse packages become more and more regular, until the laser executes RPP, such as the one depicted in Fig. 6. The rf spectrum of this trajectory matches very well to the one shown in Fig. 4(h). Finally, as the phase is further decreased through one cycle, the laser settles to a stable operation on the MGM and the rf spectrum exhibits no frequency peaks as in Fig. 4(i). Notice that the steady state overlaps with the PP (and also the RPP) over a substantial region of the feedback phase. This is the result of hysteresis between the PP and the MGM. This type of transition was also detected experimentally, and we will come back to it in the following section.

Finally, in Fig. 8, we depict the dependence of the frequency of the envelope on the pumping current. All the parameters are kept at their original values, except we set $C_p=-1.373$ and $\eta=0.135$. The points marked with full squares are the numerically computed points and the line corresponds to the linear fit. This linear dependence on pumping clearly reproduces very well the experimentally obtain dependence shown in Fig. 3.

IV. BIFURCATION ANALYSIS

The question we will address now is what structures in phase space are involved in the transition of the dynamics from simple output to RPP and back, as the feedback phase is changed. To this end, we use new tools from bifurcation theory for DDEs, in particular, the computation of one-dimensional unstable manifolds of ECMs of saddle type. We work with the Lang-Kobayashi equations in the form of Eqs. (A1) and (A2) with the values of the parameters given in Table I; see the Appendix for details. The external round-trip time was set to $\tau=0.22$ ns corresponding to an external cavity of about 3.3 cm, which is well within the short cavity regime. At the same time there are only a limited number of ECMs for any value of the feedback phase C_p, facilitating our bifurcation study.

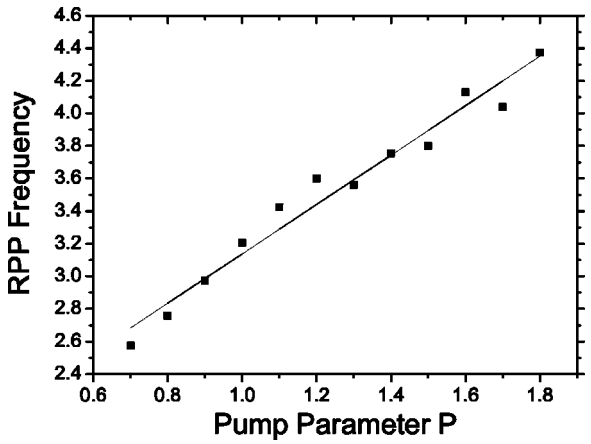

FIG. 8. Frequency of the RPP as a function of the pumping current P. The parameter values are $T=1710$, $\alpha=5.0$, $\tau=70$, $C_p=-1.373$, and $\eta=0.135$.

Figure 9 shows, in panels (a) and (b), that for the chosen parameters there is good correspondence between measured and simulated RPPs. Notice that each individual pulse package is shorter (has less peaks) compared to Fig. 6. The second, boldfaced pulse package in Fig. 9(b) corresponds to the trajectory shown in Fig. 9(c) as a projection onto the (R,N) plane, where R is the amplitude of the electric field $E=Re^{i\phi}$. This trajectory consists of an initial reinjection into a region of higher gain (lower N), which it leaves again at the end of the pulse package. The trajectory does not closeup, but the begin and end points are quite close together, so that the next pulse package is quite similar.

It is the aim of this section to study in more detail the nature of the reinjection mechanism, which, in the region of RPP, appears to provide a narrow channel in phase space back to the high-gain region. The crosses and circles in Fig.

TABLE I. Parameters of Eqs. (A1) and (A2). The parameters have been rescaled by the carrier decay rate $\gamma=1$ ns^{-1}. Hence, γ_0, Γ_{M0}, κ_0, and J_0 are in multiples of 1 ns^{-1} and τ_0 is in multiples of 1 ns.

Symbol	Meaning	Value
α	Linewidth enhancement factor	3.5
γ_0	Carrier decay rate	1.0
Γ_{M0}	Cavity decay rate	0.55
κ_0	Feedback strength	25.0
τ_0	Feedback time	0.22
G_{M0}	Proportional to small signal gain	50.0
G_{N0}	Proportional to small signal gain	0.05
J_0	Pumping current	8.0
N_N	Inversion at threshold	5.0

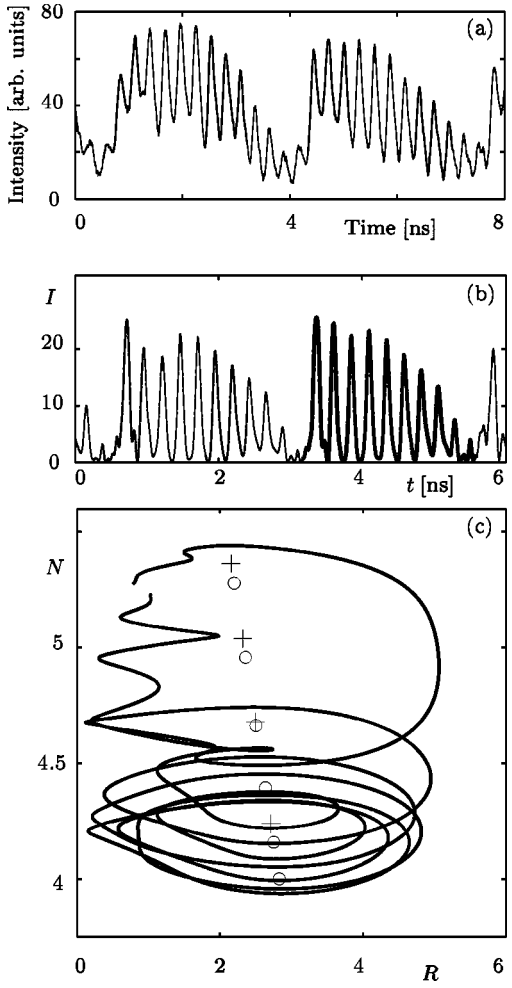

FIG. 9. Experimental (a) and simulated (b) time series of the intensity in the RPP regime. The ''basic period'' of the RPP, shown boldfaced in panel (b), corresponds to a trajectory in the (R,N) plane (c) with exactly one global reinjection from the low-gain region. Here, $C_p=31.49$ and the other parameters are as in Table I.

9(c) correspond to ECMs of the LK equation, and we will study how they are involved in (the creation of) the RPP.

A. ECMs of the LK equations

The Lang-Kobayashi equations are delay differential equations with a single fixed delay τ; see Refs. [7,8] for more details on the theory of DDEs. It is important to realize that the *phase space* of the LK equations is the infinite-dimensional space of continuous functions over the delay interval $[-\tau,0]$ with values in (E,N)-space. This is so because in order to determine the future dynamics one needs to prescribe as initial condition an entire history, namely, a point in phase space of the form $q:[-\tau,0]\rightarrow\{(E,N)\}$. The evolution of such a point q can be computed effectively by numerical integration of the equations.

The LK equations are invariant under the symmetry operation $E\rightarrow Ee^{i\Phi}$, where Φ is a constant; see Ref. [31]. Physically, this means that the solutions do not depend on the absolute phase of the optical field. As a result, the image of any solution of Eqs. (1) and (2) or Eqs. (A1) and (A2) under a rotation over Φ is again a solution.

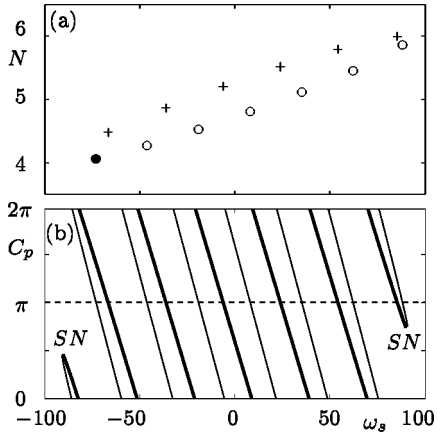

FIG. 10. Ellipse of modes (○) and antimodes (+) in the (ω_s,N) plane (a); the black dot indicates the MGM. The mode-antimode pair can be continued from creation to annihilation in the 2π-periodic parameter C_p (b); the boldfaced curve corresponds to antimodes. The modes and antimodes in (a) correspond to the value of $C_p=\pi$ indicated by the dashed line in (b). The other parameters are as in Table I.

The basic solutions of the LK equations are the ECMs that have the form $(R_se^{i\omega_st},N_s)$, that is, they are characterized by constant N_s and R_s, while they move with constant frequency ω_s. Notice that ECMs are perfectly circular periodic orbits in (E,N)-space. In light of the symmetry property of the LK equations, it is most useful to consider the dynamics in projection onto the (R,N) plane, where the ECMs appear as fixed dots. The constants R_s, ω_s, and N_s can be found as solutions of Eqs. (A5)–(A7), given in the Appendix.

For any fixed value of C_p, there are finitely many ECMs that lie on an ellipse; see Fig. 10(a). A basic stability analysis shows that the ECMs at the top of the ellipse are always saddles, also called antimodes, whereas the lower ECMs, also called the modes, are created (as C_p changes) as attractors and then lose their stability in Hopf bifurcations; see, for example, Ref. [21]. As mentioned earlier, C_p is a 2π-periodic parameter, which means that when C_p is decreased over an interval of 2π then one gets back the exact same set of ECMs. However, all ECMs will have moved to their respective direct neighbors in the lower-gain direction. When we follow the ECMs as a function of C_p over several cycles of 2π, then we see that the ECMs are created and destroyed in saddle-node bifurcations. This is shown in Fig. 10(b), which was computed by numerically solving the transcendental equations (A5)–(A7).

B. Unstable manifolds of the ECMs

We now take the view of following a single ECM over several periods of C_p from its appearance to its disappearance in saddle-node bifurcations. To this end, we plot in Fig. 11(a) the value of ω_s as a function of C_p, where C_p now runs over as many periods as it takes from the first to the second saddle-node bifurcation. Along the middle branch the

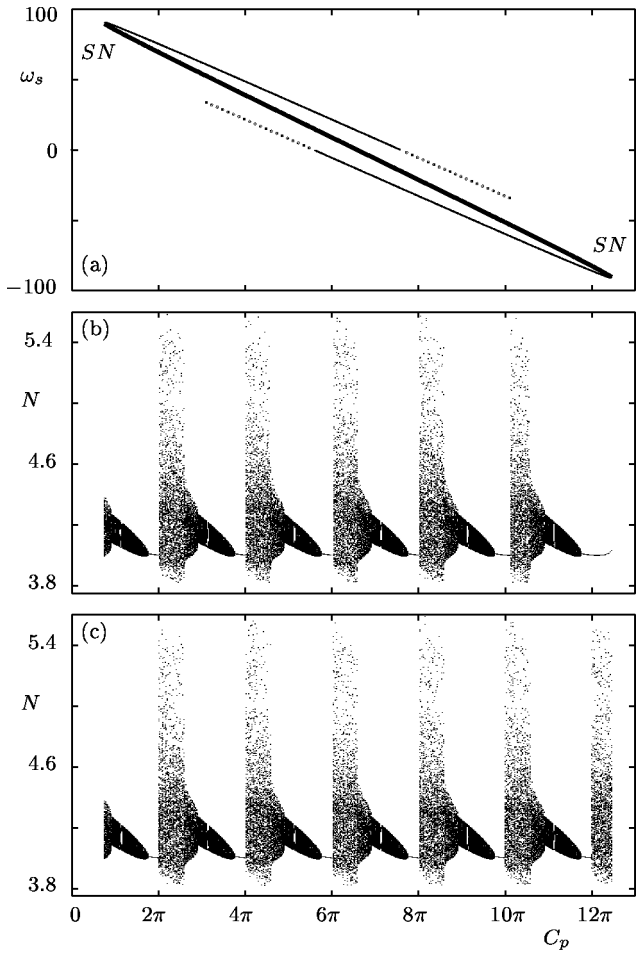

FIG. 11. Continuation of the mode-antimode pair from creation to annihilation ''unwrapped'' and plotted over its entire range of phase C_p (a), and intersections of the attractors (b) and (c) to which the first and second branch, respectively, of the (strong) unstable manifold of the saddle point antimode and thick curve in (a) converge to. The other parameters are as in Table I.

ECM is of saddle type, while it is a node on the other two branches. The dots indicate that the branches could be continued further back to the next set of saddle-node bifurcations. Mathematically, Fig. 11(a) shows the covering of Fig. 10(b).

Our next step is to compute the one-dimensional (1D) unstable manifold of the saddle-type ECM of the entire middle branch. In view of the 2π periodicity of C_p, this is equivalent to (but more convenient than) computing the 1D unstable manifolds of all ECMs over a single period of C_p. Taking the symmetry of the LK equations into account, computing a 1D unstable manifold of an ECM is of the same difficulty as computing that of an equilibrium of a DDE without symmetry. As is explained in Refs. [16,17], we can do this by integrating from the two separate starting conditions $q \pm \delta v$ (one for each branch). Here, q is a history of the ECM, v is the unstable eigendirection (over the interval $[-\tau,0]$), and δ is sufficiently small. The vector v is found by a power method; see Ref. [16]. Again it is convenient to project the manifold, which is a one-dimensional curve in phase space, onto the (R,N) plane. Due to this projection the 1D manifolds may have self-intersections.

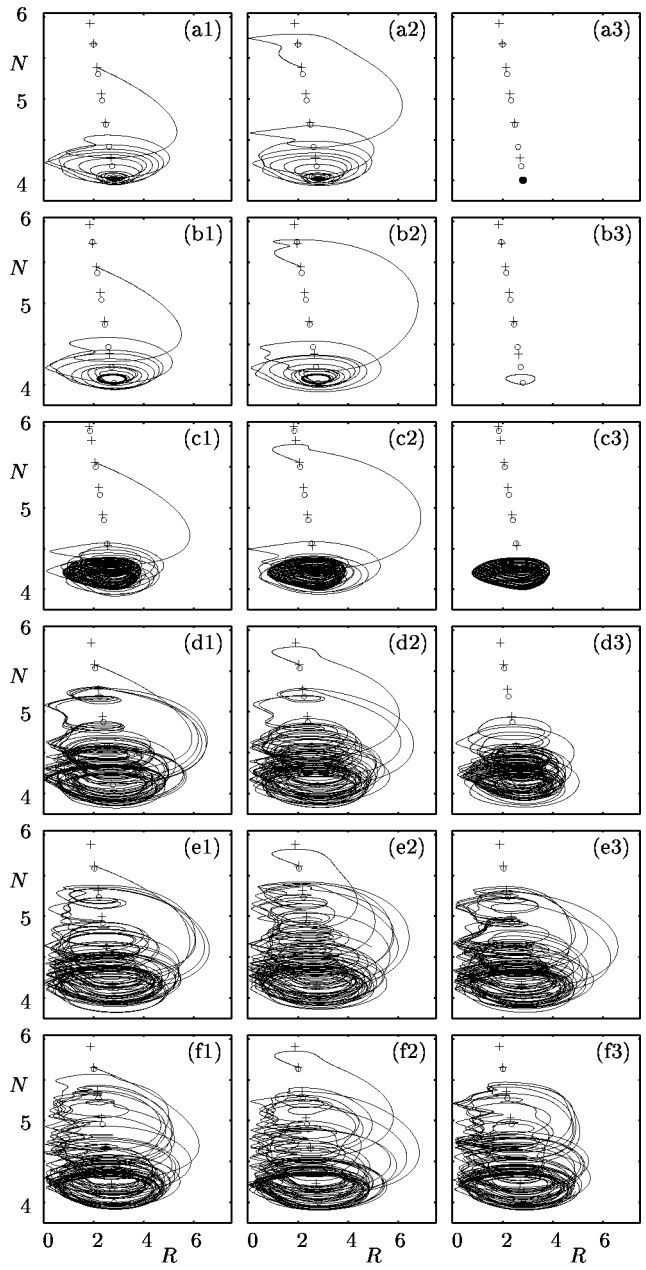

FIG. 12. Changes of the dynamics when C_p varies over 2π through a typical ''bubble.'' Shown are the first branch (first column) and the second branch (second column) of the (strong) unstable manifold of the saddle, and the attractor they go to (third column). From (a) to (f) C_p takes the values 18.46, 17.20, 14.92, 14.37, 13.51, and 12.72; the other parameters are as in Table I.

In Figs. 11(b) and 11(c), we show to which attractor each branch of the unstable manifold of the saddle ECMs of panel (a) ends up when C_p is varied in the covering space, that is, over the interval [2.36,39.11] from the creation to its disappearance in the two saddle-node bifurcations SN. We plot only the N values of the respective attractor taken whenever the trajectory crosses the section $\Sigma = \{\mathrm{Im}(E)=0, \mathrm{Re}(E)>0\}$; see also Ref. [31]. Figure 11 provides an overall picture of the dynamics, much like a bifurcation diagram, but

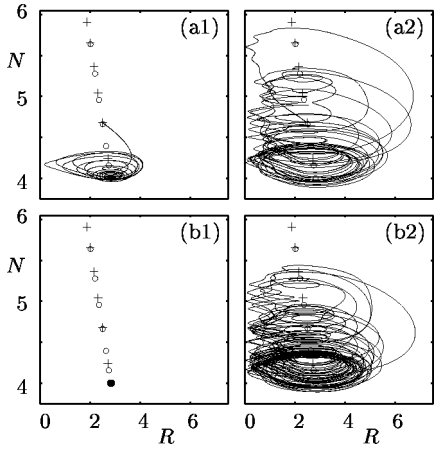

FIG. 13. Bistability region near the MGM: The two branches of the unstable manifold of one saddle ECM, shown in panels (a1) and (a2), converge to the MGM (b1) and the RPP attractor (b2), respectively. Here, $C_p = 31.494$ and the other parameters are as in Table I.

we stress that we did not follow any specific attractor. In particular, there is no hysteresis in panels (b) and (c) when C_p is scanned up or down.

The overall picture is that of ''bubbles'' consisting of a transition from a stable ECM via extra bifurcations to more complex dynamics and suddenly back to a stable ECM. It is an immediate observation that for certain values of C_p, the respective branches of the unstable manifolds of all saddle ECMs end up at the MGM. In other words, compared to the numerical bifurcation diagrams in Sec. III, we obtain the additional information that the MGM is accessible from very large regions of phase space. As a consequence, one expects stable laser output independently of the initial condition.

Furthermore, it appears that both branches of the unstable manifold end up at the same attractors for most saddles, notably those in the lower-gain region. (As we will point out below, there are, nevertheless, important differences in the transients of the two branches.) However, there is a distinctive bistability between the MGM and the PP, but only the higher-gain saddles pick this up in the sense that the two branches of their unstable manifold converge to these two different attractors; see already Fig. 13.

C. Bifurcations over one feedback phase cycle

We now consider what happens during a typical transition through one of the ''bubbles'' in Fig. 11 (we use the range $C_p \in [4\pi, 6\pi]$). To this end, we plot in Fig. 12 both branches of the (strong) unstable manifold (columns 1 and 2) and the attractor at which they end up (column 3) in the section Σ. (The possibility that the two branches end up at different attractors is discussed below.)

We start from the situation that both branches of $W^u(q)$ eventually end up at the MGM [Fig. 12(a)]. As C_p is decreased, a Hopf bifurcation takes place [Fig. 12(b)] and the laser now produces periodic output. When decreasing C_p further, a torus bifurcation (or Neimark-Sacker bifurcation) takes place, so that, after transients, both branches settle down to an attracting torus, corresponding to quasiperiodic (or very high-period locked) dynamics [Fig. 12(c)]. Upon decreasing C_p further, the torus starts to breakup into a chaotic attractor [Fig. 12(d)]. The attractor itself is localized in (confined to) a part of the high-gain region. For certain ranges of C_p, the dynamics on the breaking-up torus may be locked to lower-period periodic orbits.

It is an important observation that the second branch of the unstable manifold initially moves away from the respective attractor and only reaches it after a global reinjection starting in the low-gain region. In Figs. 12(a)–12(d), the first branch never displays global reinjection, but goes to the attractor immediately. This situation changes dramatically in a global bifurcation that is marked in Fig. 11 by a sudden increase in the size of the attractor. The localized chaotic attractor hits the stable manifold of the saddle immediately above it [Fig. 12(d)]. After this bifurcation, the dynamics can leave the previous region of localization to make a large excursion ending with a global reinjection. As can be seen in Fig. 12(e), the dynamics essentially follows the first branch of the unstable manifold during the reinjection phase. This global bifurcation is, hence, identified as an *interior crisis* [32]; the size (and nature) of the attractor suddenly changes. The chaotic attractor of Fig. 12(d) collides with a chaotic saddle, resulting in the much larger chaotic attractor in Fig. 12(e). The chaotic saddle is now part of the new attractor. An important ingredient of this bifurcation is the presence of the reinjection mechanism. Without reinjection the dynamics would never return to the high-gain region. After the interior crisis, the dynamics is of a typical form and it displays intermittency because the dynamics stays near the previous localized attractor for long periods of time interrupted by sudden large excursions.

As C_p is decreased away from the interior crisis, these large excursions become more frequent until the dynamics moves more uniformly over this large new chaotic attractor [Fig. 12(f)]. This is recognized as the RPP dynamics from Ref. [23]; see also Fig. 2. The RPP become more and more regular and eventually disappear suddenly in a second global bifurcation. This bifurcation is a *boundary crisis* [32], in which the attractor hits its basin boundary and suddenly disappears. Indeed, we found the typical long chaotic transients associated with this bifurcation before the system settles down to the MGM.

For topological reasons the boundary crisis must be preceded by a region of bistability between the RPP and the MGM. This region is very small in the ''typical'' transition studied here, but becomes very prominent near the maximum-gain region. As is to be expected, immediately after the saddle-node bifurcation creating the MGM and the saddle, one branch of the unstable manifold goes directly to the MGM. However, for a certain range of C_p the other branch converges to the large RPP attractor, while the other still ends up at the MGM. This bistability is illustrated in Fig. 13. The bistability is largest when one follows the unstable manifold of the highest-gain saddle, as is already clear in the region of $C_p \geqslant 12\pi$ in Fig. 11.

V. CONCLUSION

We have provided a detailed overview over the dynamics and the underlying mechanisms in the emission of a semi-

conductor laser being subjected to feedback from a short external cavity. We have demonstrated that the feedback phase C_p is a crucial parameter. When changing C_p over 2π, we observed experimentally a transition from stable output via periodic and quasiperiodic output to pulse packages and back to stable output. The pulse packages are regular (RPP regime) in a certain range of C_p values and can coexist with the MGM.

To analyze these experimental observations, we modeled the system with the Lang-Kobayashi equations and achieved good agreement of the obtained dynamical states and the bifurcation diagrams with the experiments. The remarkable linear scaling of the RPP frequency with the pumping current has been confirmed numerically. Furthermore, we studied the underlying structure of RPP and the transition to them by computing the 1D unstable manifolds of the saddle-type ECMs (antimodes). This revealed global bifurcations in the transition to RPP, which are characterized as an attractor featuring reinjection along a narrow ''channel'' in phase space to a region of high gain. The narrower this channel, the more regular the pulse packages.

The combination of experiment, modeling, and bifurcation analysis provides unprecedented insight into the dynamics in the short cavity regime. This was helped by the fact that there are only a small number of ECMs present. We have the hope that our approach can be extended to longer cavities with more and more ECMs, with the goal of understanding the bifurcations and dynamics involved in the complicated LFF dynamics. Previous results, for example, in Refs. [21,33,34], are consistent with the idea that global reinjection plays a central role in (the onset of) LFF. However, this detailed study of the LFF phenomenon is still a considerable challenge, as the techniques used here represent the state of the art.

The combination of methods used here might be of model character for the study of other systems with delay which are currently the focus of interest, in particular, mutually coupled lasers, unidirectionally coupled laser systems, and lasers with phase-conjugate or optoelectronic feedback.

APPENDIX

The Lang-Kobayashi equations [24] that model the feedback coherent of the laser radiation from an external cavity are are given as

$$\frac{dE}{ds}=\frac{1}{2}G_{\mathrm{M0}}(1+i\alpha)[N(s)-N_N]E(s) + \kappa_0 E(s-\tau_0)\exp[-iC_p], \tag{A1}$$

$$\frac{dN}{ds}=J_0-\gamma_0 N(s)-[\Gamma_{\mathrm{M0}}+G_{\mathrm{N0}}(N(s)-N_N)]|E(s)|^2, \tag{A2}$$

for the electric field E and the inversion N. Equations (A1) and (A2) are nondimensional: time is measured in multiples of the carrier lifetime γ, which was set to $\gamma=1$ ns. The various physical parameters in these equations are given in Table I, together with their values used in the bifurcation studies of Sec. IV.

The phase of the reinjected field is given by $C_p=\omega_0\tau_0$, where ω_0 is the frequency of the solitary laser. Clearly, the phase can be varied by either changing the frequency of the laser or the length of the external cavity.

Equations (A1) and (A2) can be further simplified and the number of necessary parameters reduced to six as follows. We introduce the rescaled electric field A and inversion X by

$$X=\frac{G_{\mathrm{M0}}}{2\gamma_p}(N-N_{\mathrm{N}}), \quad A=\sqrt{\frac{E_{\mathrm{M}}^2 G_{\mathrm{N0}}}{2\gamma_0}}E,$$

where $\gamma_{\mathrm{p}}=\Gamma_{\mathrm{M0}}G_{\mathrm{M0}}/G_{\mathrm{N0}}$ is the rescaled cavity lifetime, still measured in multiples of $\gamma=1$ ns. By rescaling time as $t=\gamma_{\mathrm{p}}s$, we obtain the equations

$$\frac{dA}{dt}=(1+i\alpha)AX+\eta A(t-\tau)e^{-iC_{\mathrm{P}}}, \tag{A3}$$

$$T\frac{dX}{dt}=P-X-(1+2X)|A|^2. \tag{A4}$$

Equations (A3) and (A4) are Eqs. (1) and (2) from Sec. III, after the convenient renaming of A and X back to E and N. The new parameters are related to the parameters in Table I as follows: $P=(G_{\mathrm{M0}}/2\gamma_{\mathrm{p}}\gamma_0)(J_0-\gamma_0 N_{\mathrm{N}})$ is the pumping current above threshold, $T=\gamma_{\mathrm{p}}/\gamma_0$ is the ratio of cavity lifetime to carrier lifetime, $\eta=\kappa_0 G_{\mathrm{N0}}/G_{\mathrm{M0}}\Gamma_{\mathrm{M0}}$ is the rescaled feedback strength, and $\tau=\gamma_{\mathrm{p}}\tau_0$ is the external delay in terms of the rescaled time. For the parameter values in Table I, we have $P=0.136$, $T=550$, $\eta=0.0455$, $\tau=121$, and $\alpha=3.5$.

The basic solutions of the LK equations are the ECMs. By inserting the ansatz $(R_s e^{i\omega_s t},N_s)$ into Eqs. (A1) and (A2), one obtains the following set of transcendental equations:

$$\omega_s=-\alpha\kappa_0\left[\cos(\omega_s\tau+C_p)+\frac{1}{\alpha}\sin(\omega_s\tau+C_p)\right], \tag{A5}$$

$$N_s=N_N-\frac{2\kappa}{G_{\mathrm{M0}}}\cos(\omega_s\tau+C_p), \tag{A6}$$

$$R_s=\left\{\frac{J_0-\gamma_0 N_s}{(\Gamma_{\mathrm{M0}}+G_{\mathrm{N0}}(N_s-N_N))E_M^2}\right\}^{1/2}. \tag{A7}$$

For given values of the parameters, these equations can be solved numerically by solving for the constants ω_s, N_s, and R_s in this order.

[1] D. Lenstra, B.H. Verbeek, and A.J. den Boef, IEEE J. Quantum Electron. **21**, 674 (1985).
[2] C.R. Mirasso, P. Cole, and P. Garcia-Fernandez, IEEE Photonics Technol. Lett. **8**, 299 (1996).
[3] V. Annovazzi-Lodi, S. Donati, and A. Scire, IEEE J. Quantum Electron. **33**, 1449 (1997).
[4] J. Ohtsubo, Opt. Rev. **6**, 1 (1999).
[5] I. Fischer, Y. Liu, and P. Davis, Phys. Rev. A **62**, 011801(R) (2000).
[6] IEEE J. Quantum Electron. **38** (2002), feature section on optical chaos and applications to cryptography.
[7] J.K. Hale and S.M. Verduyn Lunel, *Introduction to Functional Differential Equations*, Applied Mathematical Sciences, Vol. 99 (Springer, New York, 1993).
[8] O. Diekmann, S.A. van Gils, S.M. Verduyn Lunel, and H.O. Walther, *Delay Equations: Functional-, Complex-, and Nonlinear Analysis* (Springer, New York, 1995).
[9] S.M. Verduyn Lunel and B. Krauskopf, in *Nonlinear Laser Dynamics: Concepts, Mathematics, Physics, and Applications International Spring School*, edited by Bernd Krauskopf and Daan Lenstra, AIP Conf. Proc. No. 548 (AIP, Melville, NY, 2000), p. 66.
[10] H. Glüsing-Lüerssen, SIAM J. Control Optim. **35**, 480 (1997).
[11] C.M. Marcus and R.M. Westervelt, Phys. Rev. A **39**, 347 (1989).
[12] J.D. Murray, *Mathematical Biology, Biomathematics Texts* (Springer-Verlag, Berlin, 1980), Vol. 19.
[13] K. Engelborghs, DDE-BIFTOOL: a MATLAB package for bifurcation analysis of delay differential equations, available at http://www.cs.kuleuven.ac.be/~koen/delay/ddebiftool.shtml
[14] D. Pieroux, T. Erneux, T. Luzyanina, and K. Engelborghs, Phys. Rev. E **63**, 036211 (2001).
[15] D. Pieroux, T. Erneux, B. Haegeman, and K. Engelborghs, Phys. Rev. Lett. **87**, 193901 (2001).
[16] K. Green and B. Krauskopf, Phys. Rev. E **66**, 016220 (2002).
[17] B. Krauskopf and K. Green, J. Comput. Phys. **186**, 230 (2003).
[18] K. Green, B. Krauskopf, and K. Engelborghs, Physica D **173**, 114 (2002).
[19] K. Green and B. Krauskopf Int. J. Bifurcation Chaos Appl. Sci. Eng. (to be published); http://www.enm.bris.ac.uk/anm/preprints/2002r06.html
[20] *Nonlinear Laser Dynamics: Concepts, Mathematics, Physics, and Applications International Spring School* (Ref. [9]).
[21] G.H.M. van Tartwijk and G.P. Agrawal Prog. Quantum Electron. **22**, 43 (1998).
[22] I. Fischer, T. Heil, and W. Elsäßer, in *Nonlinear Laser Dynamics: Concepts, Mathematics, Physics, and Applications International Spring School* (Ref. [9]), p. 218.
[23] T. Heil, I. Fischer, W. Elsäßer, and A. Gavrielides, Phys. Rev. Lett. **87**, 243901 (2001).
[24] R. Lang and K. Kobayashi, IEEE J. Quantum Electron. **16**, 347 (1980).
[25] D.W. Sukow, T. Heil, I. Fischer, A. Gavrielides, A. Hohl-AbiChedid, and W. Elsäßer, Phys. Rev. A **60**, 667 (1999).
[26] T. Heil, I. Fischer, W. Elsäßer, J. Mulet, and C.R. Mirasso, Opt. Lett. **24**, 1275 (1999).
[27] G. Vaschenko, M. Guidici, J.J. Rocca, C.S. Menoni, J.R. Tredicce, and S. Balle, Phys. Rev. Lett. **81**, 5536 (1998).
[28] A. Uchida, Y. Liu, I. Fischer, P. Davis, and T. Aida, Phys. Rev. A **64**, 023801 (2001).
[29] M. Pan, B. Shi, and G.R. Gray, Opt. Lett. **22**, 166 (1997).
[30] M. Peil, T. Heil, I. Fischer, and W. Elsäßer, Phys. Rev. Lett. **88**, 174101 (2002).
[31] B. Krauskopf, G.H.M. van Tartwijk, and G.R. Gray, Opt. Commun. **177**, 347 (2000).
[32] C. Robert, K.T. Alligood, E. Ott, and J.A. Yorke, Physica D **144**, 44 (2000).
[33] T. Sano, Phys. Rev. A **50**, 2719 (1994).
[34] R.L. Davidchack, Y.C. Lai, A. Gavrielides, and V. Kovanis, Physica D **145**, 130 (2000).